IEEE Access
Multidisciplinary ⋮ Rapid Review ⋮ Open Access Journal

Received 3 May 2024, accepted 25 May 2024, date of publication 3 June 2024, date of current version 17 September 2024.

Digital Object Identifier 10.1109/ACCESS.2024.3408797

RESEARCH ARTICLE

Quantifying the Earthquake Risk to the Electric Power Transmission System in Los Angeles at the Census Tract Level

BOYU CHENG[1], LINDA NOZICK[1], (Member, IEEE), IAN DOBSON[2], (Life Fellow, IEEE), RACHEL DAVIDSON[3], DENIS OBIANG[4], JOSÉ DIAS[4], (Member, IEEE), AND MICHAEL GRANADOS[4]

[1]School of Civil and Environment Engineering, Cornell University, Ithaca, NY 14850, USA
[2]Electrical and Computer Engineering Department, Iowa State University, Ames, IA 50011, USA
[3]Civil and Environment Engineering Department, University of Delaware, Newark, DE 19716, USA
[4]Los Angeles Department of Water and Power, Los Angeles, CA 90012, USA

Corresponding authors: Boyu Cheng (bc652@cornell.edu), Linda Nozick (lkn3@cornell.edu), and Ian Dobson (dobson@iastate.edu)

This work was supported by NSF under Grant 1735354 and Grant 2153163.

ABSTRACT This paper develops a probabilistic earthquake risk assessment for the electric power transmission system in the City of Los Angeles. Via a dc load flow analysis of a suite of damage scenarios that reflect the seismic risk in Los Angeles, we develop a probabilistic representation for load shed during the restoration process. This suite of damage scenarios and their associated annual probabilities of occurrence are developed from 351 risk-adjusted earthquake scenarios using ground motion that collectively represent the seismic risk in Los Angeles at the census tract level. For each of these 351 earthquake scenarios, 12 damage scenarios are developed that form a probabilistic representation of the consequences of the earthquake scenario on the components of the transmission system. This analysis reveals that substation damage is the key driver of load shed. Damage to generators has a substantial but still secondary impact, and damage to transmission lines has significantly less impact. We identify the census tracts that are substantially more vulnerable to power transmission outages during the restoration process. Further, we explore the impact of forecasted increases in penetration of residential storage paired with rooftop solar. The deployment of storage paired with rooftop solar is represented at the census tract level and is assumed to be able to generate and store power for residential demand during the restoration process. The deployment of storage paired with rooftop solar reduces the load shed during the restoration process, but the distribution of this benefit is correlated with household income and whether the dwelling is owned or rented.

INDEX TERMS Power transmission systems, resilience, reliability, earthquake, equity, solar power.

I. INTRODUCTION

Earthquakes can cause extensive damage to components of electric power systems, including substations, generation plants, and transmission lines, causing hardships to customers and inhibiting the response process. For instance, approximately 2.5 million people experienced power outages during the 1994 Northridge earthquake in Los Angeles [1]. About 50% of 66 kV cables, 15% of 11 kV cables, and 4 substations were damaged after the 2011 earthquake in Christchurch, New Zealand [2]. In 2016, the Fukushima earthquake caused a serious power blackout in the Tokyo area [3].

The Los Angeles area has experienced several significant earthquakes with the most recent being the 5.1 magnitude La Habra earthquake that occurred in 2014 and that only caused momentary service interruption. This event contrasts with the 1994 Northridge earthquake that caused widespread power outages as far away as British Columbia. Los Angeles is the second largest city in the United States with about 4 million residents; therefore, it is important to understand the seismic resiliency of the Los Angeles power transmission system.

The associate editor coordinating the review of this manuscript and approving it for publication was Ali Raza.

Over the past decade, the global deployment of solar Photovoltaic (PV) technology has risen significantly [4]. In Los Angeles in particular, the adoption of customer-owned solar and storage is a key element of the goal of Los Angeles to transition fully to renewables by 2045. The integration of customer-owned solar and storage could have a significant impact on the power system [5], including its resilience to earthquakes.

This paper develops a stochastic characterization of the load shed in Los Angeles based on the earthquake hazard in the area. Additionally, the impact of the adoption of customer-owned solar and storage on the resilience of the power system to earthquake hazards is analyzed. In this paper, the power transmission system of Los Angeles is represented by a dc load flow model representing substations, generation plants, and transmission lines. The earthquake hazard is characterized by 351 earthquake scenarios generated by Soleimani et al. [6]. Those events combined with their annual probabilities of occurrence match the regional hazard. Each earthquake scenario is used to develop a suite of damage scenarios, each of which translates the earthquake scenario into a realization of the damage to the transmission system that could result from the occurrence of that earthquake scenario. The evolution of rooftop solar and storage penetration is given by the LA100 study [5], which provides predictions of rooftop solar and storage adoption in 2030 at the census tract level. In this study, we only consider residential storage paired with rooftop solar since the rooftop solar without storage will be disconnected during an outage [7]. The LA 100 study was a technical feasibility study to identify potential investment pathways to achieve a power system that operates with no carbon-based energy sources by 2045 in Los Angeles. When residential storage is paired with rooftop solar (solar plus storage), it acts to satisfy residential demand, reducing the demand on the power company, thus allowing the power grid to supply less power without shedding load. It is assumed that the residential rooftop solar plus storage is not damaged by the earthquake [8] and is sized to supply all the residential demand of that customer.

The dc load flow model for the restoration process for each damage scenario assumes geographically distributed power demands reflective of an event that strikes in June 2030 and for which the restoration period extends until August 2030; hence the earthquake is assumed to occur during peak seasonal demand.

HAZUS is a risk modeling tool for natural hazards including earthquakes, hurricanes, floods, and tsunamis that has been developed by the Federal Emergency Management Agency (FEMA) [9]. We adopt its assumptions as to the cadence of the restoration process for electric power systems. More specifically, the assumptions we adopt as to the restoration process for the electric power transmission system includes the 9 time periods as defined in the HAZUS methodology, and after each period, a set of component types by the severity of damage are assumed to be repaired. The dc load flow problem is run for each damage scenario and time period, identifying by substation the amount of power delivered. The resulting load delivered to each substation is then distributed to each census tract in Los Angeles via parameters that specify how the delivered load at a substation is allocated to the associated census tracts. It is assumed that the consumption is constant across individuals within a census tract during each hour of the restoration process.

This study makes contributions along two main thrusts:

1. The study quantifies the impact of the earthquake risk on the census tracts of Los Angeles due to damage to the transmission system. In addition to its value as a case study, it extends earthquake hazard analysis of transmission systems to the probabilistic load shed at the census tract level to reveal the differing geographic impacts across the city. Since damage to the transmission lines, transmission substations and generation plants are all considered, we can confirm that damage to the substations is the key driver for the load shed in Los Angeles. The worst-case earthquake timing is at the summer peak demand; the load shed reduces proportionally for earthquakes in the spring.
2. The study quantifies the positive impacts of future residential solar plus storage in power system restoration after an earthquake at the census tract level, showing these differing impacts across the city. We find that the benefits are not uniform across income classes: after an earthquake, the predicted rooftop solar plus storage deployments tend to benefit census tracts with wealthier citizens who own their homes.

The remainder of this paper is organized as follows. The second section describes the relevant literature. The third section gives the formulation of the models used in this study. The fourth section describes the case study. The last section provides concluding remarks.

II. LITERATURE REVIEW

Several studies explore the impact of earthquakes on power systems. One direction of inquiry is focused on the vulnerability of the components of the power system and investments in those components to mitigate earthquake risk [10], [11], [12], [13], [14], [15], [16]. Another direction in the literature is focused on the performance of the power system under earthquake hazards [17], [18], [19], [20], [21], [22], [23], [24]. Because this study is focused on earthquake resilience of the power transmission system in the Los Angeles area, which is administered by the Los Angeles Department of Water and Power (LADWP), it is worthwhile to review the key previous studies conducted in this area. Shinozuka et al. [25] compared the performance of the LADWP's transmission network using 47 earthquake scenarios. The risk curves were also developed. Çağnan et al. [26] developed a discrete-event-simulation model to analyze the restoration of the power system in Los Angeles after earthquakes. The analysis contained three parts. In the first part, the seismic hazard was defined by identifying 47 earthquake

scenarios and their hazard-consistent annual occurrence probabilities. In the second part, 600 initial damage states of transmission substations were generated by Monte Carlo simulation under those 47 earthquake scenarios and the initial functionality data for each scenario were obtained. In the third part, the restoration process was simulated using a restoration model based on the data gathered by LADWP which used damage states and initial functionality as inputs. The results showed that outages could exist for up to 10 days. The results also showed geographic variation of the annual probability of outages with the duration longer than 3 and 24 hours based on the service zones. Shinozuka et al. [27] studied the seismic performance of the power transmission system in the Los Angeles area. Only components in substations were considered to experience earthquake damage. Xu et al. [28] focused on the optimization of the scheduling of the restoration tasks for the power system in Los Angeles after earthquake events. A stochastic integer program was developed to schedule the restoration tasks to minimize the average outage time for each customer. Sarreshtehdari et al. [29] used the Los Angeles power system as the test case for measuring the post-earthquake performance of electric networks using a streamlined approach.

The studies of the impact of earthquake on the power grid with rooftop solar and storage system are more limited. With regard to damage to rooftop solar panels by earthquakes, Ding et al. [30] conducted seismic simulations via Finite Element Analysis of home rooftop photovoltaic systems. They found that the exposure of bare metal wire to ambient conditions and electrical lead short circuit were the main sources of damage. Walters et al. [31] utilized empirically driven friction coefficients and ground motion assumptions for seven western U.S. states to evaluate the potential seismic displacement between an isolated rooftop PV array and the roof of the supporting building. The results suggested that the isolated rooftop PV arrays were safe and economical. Regarding the impact of solar plus storage on the resilience of the power systems after earthquakes, Ceferino et al. [32] analyzed the improvement of post-earthquake power availability in San Carlos, California, after the adoption of rooftop solar panels by households. In their study, a Monte Carlo method was used to generate realizations of earthquake building damage, and a risk metric was defined to measure cooperation and sharing of energy during an outage. Patel et al. [33] conducted a similar study to explore how increasing the adoption of rooftop solar can improve the resilience to power outages after earthquakes. Artis et al. [34] presented a non-convex mixed-integer nonlinear four-level optimization framework to reinforce power distribution networks against earthquakes with consideration of renewable-based multi-microgrids. The components of the multi-microgrids in that study include wind turbines, photovoltaics, and energy storage systems. Another study explored the impact of solar plus storage on the resilience of power systems under general natural disasters. Galvan et al. [35] studied how rooftop solar and battery energy storage systems improve the power distribution system resilience to natural disasters. A case study was done using the IEEE 33-bus radial distribution system. The results demonstrated that rooftop solar and battery energy storage systems can provide power generation support and bus voltage improvements after natural disasters. For studies related to the resilience of power systems with general distributed energy resources, but not solar with storage, see [35], [36], and [37].

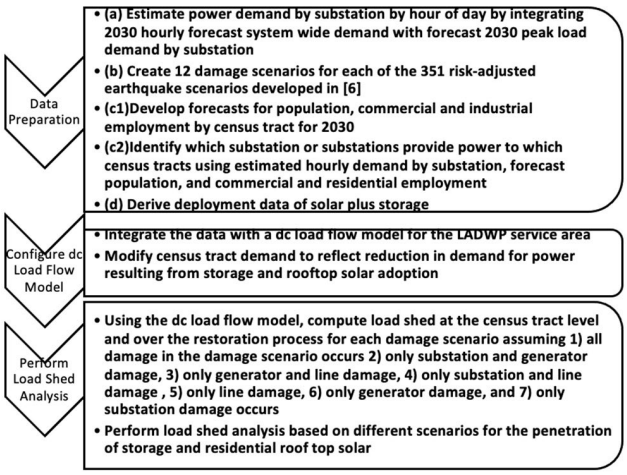

FIGURE 1. Analysis process.

This paper focuses on power outages caused by earthquakes at the census tract level. There seems to be no literature related to allocating load shed caused by earthquakes to census tracts; but there are some studies that analyzed outages caused by other natural hazards at the census tract level. For example, Guikema et al. [38] developed a hurricane power outage prediction model which predicts the fraction of the population that will lose power by the hurricane for each census tract. In that study, the number of customer meters that had outages in each grid cell was scaled to a census tract level and the model was trained on that data. Of course, hurricane damage from hurricanes is quite different than damage via earthquakes with the former more centered on transmission line damage and the later impacting substations and generating plants, which generally take substantially longer to repair. McRoberts et al. [39] used a binary classification model to predict whether a census tract had a power outage.

III. METHODOLOGY

There are two primary goals in this study. Under earthquake hazard, the first goal is to develop a stochastic characterization of the load shed in Los Angeles, and the second goal is to analyze the impact of the adoption of customer-owned solar plus storage on the resilience of power system. The modeling steps in this analysis are shown in Fig. 1.

A. DATA PREPARATION

Four types of input data are used in this analysis: (a) power transmission network and power demand at the substations,

(b) damage scenarios which represent the earthquake hazard to the physical components of the system, (c) power demand for residential, transportation, commercial and industry uses by census tract, (d) deployment data of solar plus storage.

For (a), LADWP provided a dc power transmission system network with buses, transmission lines, and transformers. Buses are connected by either transmission lines or transformers. Each bus is located at a substation or generation plant. If it is in a generation plant, the power generated by the generator will be injected at the bus. Forecasts from LADWP provide D_T^h, the year 2030 demand by hour of the day h for the system. They also provided a summer peak forecast for 2030 that gives demand by substation. We merge these datasets together to derive an estimate for demand by substation by hour for all of 2030.

For (b), since the performance of the power system depends on the joint distribution of damages to the power system components given the earthquake event, we use the optimization method developed by Brown et al. [40] to create a suite of damage scenarios which approximately match the vulnerability of each component for each of the 351 earthquake events. According to the HAZUS methodology, for each earthquake event, each power system component (substation, generation plant, and transmission line) can be in one of 5 damage states None, Slight, Moderate, Extensive, and Complete [9]. Under each damage scenario, each component falls in exactly one damage state. In this study, we generate 12 risk adjusted damage scenarios for each earthquake event to sufficiently match the component damage state probabilities based on the impact of the earthquake event by location. Each earthquake event has a hazard-consistent annual probability of occurrence, and the probability of each damage scenario is the calculated by the optimization method in [40]. Since there are 351 earthquake events, there are a total of 4,212 damage scenarios.

For (c1), demand d_{ts}^h in each hour h, census tract t, and sector s, was estimated as $d_{ts}^h = f_{st} R_s^h A^h$, where R_s^h is the proportion of study area power demand that is for sector s in hour h, A^h is the total demand across the study area in hour h, and f_{st} is the fraction of the sector s study area demand that is in census tract t. Four sectors s are considered: residential, commercial, transportation, and industrial. The LA100 study provides predictions for R_s^h, the proportion of power demand in each sector s at hour h in 2030 [5]. For residential and transportation sectors, f_{st} is estimated by the fraction of the study area population in census tract t ($f_{Rt} = p_t / \sum_t p_t$). For the commercial and industrial sectors, f_{st} is estimated by the fraction of the sector s study area employment that is in census tract t ($f_{Ct} = E_{Ct} / \sum_t E_{Ct}$).

We used different methods to predict the population and employment for each census tract in 2030. The population prediction at the census tract level is obtained using the Hamilton-Perry method [41], which predicts the population by age and sex using cohort-change ratios, which are computed from the population data in the two most recent censuses. In our case, the census data from 2010 and 2020 captured by the American community survey [42], [43] are used.

For predicting employment at the census tract level, first we categorize employment data from American community survey [44] into two categories: commercial, and industrial and other. Then we predict the employment in 2030 using the Constant Share model [45], in which, for a specific type of employment, the growth rate for that employment at each census tract matches the growth rate for that employment at the national level. That is, E_{et}^{y+n}, the employment of type e in census tract t *at year* $y+n$,is calculated by $E_{et}^{y} J_e^{y+n} / J_e^{y}$ where E_{et}^{y} is the employment of type e in census t at year y, J_e^{y} is the employment of type e nationally in year y, and J_e^{y+n} is the projected employment type e nationally in year $y+n$. In our study, y is 2020, $y+n$ is 2030, and we use the projected employment for Los Angeles County as of J_e^{2030} [46]. To test the accuracy of the Constant Share model, we applied the method to predict commercial employment and industrial and other employment in 2020 by using the 2011 employment data as base case (y is 2011, $y+n$ is 2020). Since commercial employment and industrial and other employment for each census tract has been released, we compared the predicted value with the true value for each census tract in 2020 using the percent difference. For commercial employment prediction, among the 596 census tracts in our study area, 502 have percent differences lower than 25%, 88 of them have percent difference between 25% and 50%, and 6 of them have a percent difference larger than 50%. We call these census tracts with percent difference greater than 50% outliers and for them, we extrapolate the historical trend for prediction rather than using the Constant Share model. For industrial and other employment prediction, 95 census tracts are outliers. Again, we assume that the Constant Share model is sufficient for the census tracts with prediction errors lower than 50% and use extrapolation of the historical trend for outlier census tracts [45].

For (c2), to understand the power distribution pattern from substations to census tracts, we use a capacitated transportation problem to allocate the power supplied to substations to census tracts when there has been no earthquake, where the distance between a substation and a census tract is the great circle distance between the substation and the centroid of the census tract. The power available at each substation in each hour are the power availabilities. This formulation incentivizes the supply of a census tract via the closest substation locations. The formulation is shown in (1)-(4).

$$Min \sum_h \sum_{k=1}^{M} \sum_{t=1}^{N} c_{kt} x_{kt}^h \tag{1}$$

$$\sum_{t=1}^{N} x_{kt}^h = O_k^h, \quad \forall k, h \tag{2}$$

$$\sum_{k=1}^{M} x_{kt}^h = Q_t^h, \quad \forall t, h \tag{3}$$

$$x_{kt}^h \geq 0, \quad \forall k, t, h \tag{4}$$

where x_{kt}^h is the power transferred from substation k to census tract t at hour h and c_{kt} is the great circle distance from

substation k to the centroid of census tract t. The objective is to minimize the total "cost" at hour h, which is defined by the sum of $c_{kt}x_{kt}^h$. O_k^h is power available at substation k at hour h and M is the total number of substations. Q_t^h is the load demand at census tract $t$athour$h$, and N is the total number of census tracts. By solving this transportation problem, we obtain the values x_{kt}^h, which map power available by substation to each census tract for consumption at hour h. Notice that the formulation given in (1)-(4) essentially decomposes by hour of day; that is, the solution variables are independent of each other by time period. Further, both O_k^h and Q_t^h are the result of the data preparation steps in Fig. 1 and are computed by hour of day.

In each hour, this formulation establishes which census tracts may receive power from which substations. Across all the hours of the year, for most census tracts, each census tract receives all their power from the same single substation but there are a small number of census tracts that receive power from two (almost 5% of census tracts), three (about 0.4%) or four (1 census tract) substations, and these relationships are essentially constant across each hour across the year. As we analyze the power flow under each earthquake damage scenario, we assume that these relationships are fixed. As a result, during each hour, the fraction of the power that is at substation that is delivered to a census tract is fixed based on the power flow in the absence of an earthquake event and calculated by equations (1) - (4). Hence, we do not represent any distribution system reconfiguration during the restoration process.

For (d), to explore the impact of adopting solar plus storage, we use the predicted deployment capacity of residential customer solar plus storage in the Los Angeles area given in the LA100 study. As mentioned previously, the LA100 study was conducted to understand the technical feasibility and potential investment pathways to achieve a power system that operates with no carbon-based energy sources by 2045 [5]. These predicted deployment capacities are developed by using the historical penetration rates (attachment rate) of distributed storage paired with customer rooftop solar and the historical ratios of storage capacity with customer rooftop solar capacity. Since Burbank and Glendale are not included in the LA100 study, deployment in those two areas is not considered in our study. Two scenarios of deployment that appear in the LA100 study are used in this analysis. The first scenario is referred to as SB100, which closely complies with existing California law Senate Bill 100 [47] and gives the prediction of the deployment of customer solar plus storage and is the more conservative [5]. The other scenario is called Early & No Biofuels, which is designed to achieve the goal of 100% renewable energy across the power system by 2035; ten years earlier and assumes higher levels of customer solar plus storage adoption [5]. In both scenarios, the predicted deployment capacities are at the census tract level. Some assumptions are made related to the residential customer solar plus storage in our use of these scenarios:

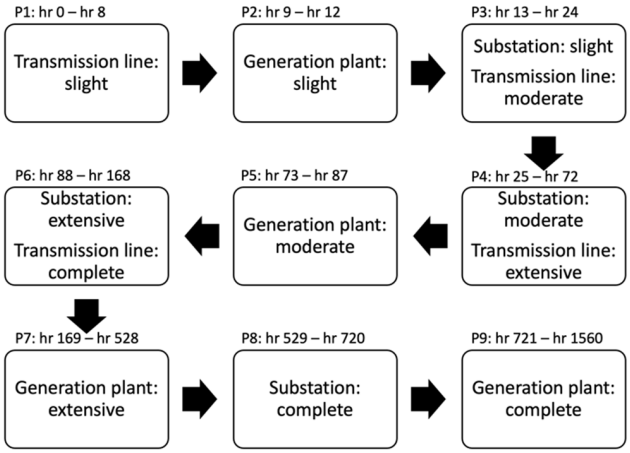

FIGURE 2. Component damage state restored by the end of each time period (format is component: damage state).

1. Since the residential rooftop solar systems are robust to earthquake [8], [30], we assume the residential customer solar plus storage is not damaged by earthquakes.
2. The residential customer solar plus storage can operate in off-grid mode during the outage which means that the solar plus storage can still generate, store, and provide power to meet the co-located residential load demand.
3. The residential customer solar plus storage only serves residential demand.
4. The residential customer solar plus storage will work at full potential, which means the maximum power it can provide in each hour is its capacity value.

B. POWER FLOW ANALYSIS

The performance of the network after earthquakes is analyzed by conducting a dc power flow analysis under each damage scenario by hour over the restoration horizon. The load shed at each substation and generation plant in each time period for each earthquake damage scenario is determined from that analysis. As in HAZUS, we assume the restoration process has 9 periods, and that functioning of certain damaged network components are restored at the end of each period, as shown in Fig. 2. For example, by the end of period 1, the repair of all transmission lines that experienced slight damage is completed. Hence, we assume in the model that, beginning in period 2, all transmission lines that experienced slight damage may be used.

Equations (5-10) provide the formulation of the dc load flow model. The objective function is to minimize the total load shed for each bus over the entire restoration process. U_i^h is the load shed in MW for bus i at hour h. (8) is the power flow constraint for each branch. B is the set of all buses. θ_i^h is the phase angle for bus i at hour h. Λ_{ij}^h is the damage state of branch (i, j), and if (i, j) is a transformer, Λ_{ij}^h is 0. $\Delta_{s_i}^h$ is the damage state of the substation or generation plant at bus i at period h. X_{ij} is the reactance of branch (i, j). P_{ij}^h is the power flow at branch (i, j) at hour h. (9) is the flow conservation

constraint for each bus. $I(i)$ are the generators connecting at bus i, if there is a generator g connected to bus i, G_g^h is the real power generated by generator g at hour h. $\delta^+(i)$ is the set of lines such that the origin bus is i, and $\delta^-(i)$ is the set of lines such that the destination bus is i. Since LADWP has interactions with other grids, inj_i^h is the external power injection at bus i. D_i^h is the demand at bus i at hour h and the load shed at bus i must be less than its demand as shown in (8). Generator capacity and branch capacity constraints are shown in equation (9) and (10). G_g^c is the capacity of generator g, $\Delta_{s_g}^h$ is the damage state of generator g at hour h, and P_{ij}^c is the capacity of branch (i, j). In (10), note that generators supply the network by radial lines, so that any reduction in generation reduces the line flow. If there is no generator at bus i then $\Delta_{s_i}^h = 0$.

$$\min \sum_{h=1}^{1560} \sum_{i \in B} U_i^h \tag{5}$$

$$(\theta_i^h - \theta_j^h)(1 - \Lambda_{ij}^h)(1 - \Delta_{s_i}^h)(1 - \Delta_{s_j}^h) = X_{ij} P_{ij}^h, \quad \forall h, (i, j) \tag{6}$$

$$\sum_{g \in I(i)} G_g^h - \sum_{(i,j) \in \delta^+(i)} P_{ij}^h + \sum_{(i,j) \in \delta^-(i)} P_{ij}^h + \text{inj}_i^h = D_i^h - U_i^h, \quad \forall h, i \tag{7}$$

$$0 \le U_i^h \le D_i^h, \quad \forall h, i \tag{8}$$

$$0 \le G_g^h \le G_g^c (1 - \Delta_{s_g}^h), \quad \forall h, g \tag{9}$$

$$\left| P_{ij}^h \right| \le P_{ij}^c (1 - \Lambda_{ij}^h)(1 - \Delta_{s_i}^h)(1 - \Delta_{s_j}^h), \quad \forall h, (i, j) \tag{10}$$

Once the load shed by census tract is computed for each hour of each day during the restoration process for each damage scenario, the probability for each earthquake event and damage scenario is used to compute the distribution of system-wide load shed.

To incorporate customer solar plus storage into the current power system network, we quantify how much load is displaced from each bus after adopting customer solar plus storage. Suppose the capacity of customer solar plus storage in census tract t is S_t and the residential demand in that census tract at hour h is $d_{t_R}^h$, as mentioned in Data Preparation (c1). If $S_t \ge d_{t_R}^h$, the new residential demand of census tract t is 0, otherwise, the new residential demand of census tract t is $d_{t_R}^h - S_t$. Let us call this new residential demand of census tract t as $d_{t_R}^h{}'$. Notice that $d_{t_R}^h{}'$ still must be served via the power grid. The difference between the original residential demand $d_{t_R}^h$ and the new residential demand $d_{t_R}^h{}'$ for census tract t is the residential demand served by solar plus storage.

After we determine the new residential demand for each census tract, we can update the new total demand for each census tract by summing the demands in four sectors. For census tract t at hour h, the new total demand $d_t^h{}' = d_{t_R}^h{}' + d_{t_T}^h + d_{t_C}^h + d_{t_I}^h$. This new total demand $d_t^h{}'$ is the demand from census tract t that still needs to be served by the power grid.

Then, we aggregate the demand from census tracts to substations. We assume the power distribution pattern from substations to census tracts we derived from the transportation problem under the network without solar plus storage stays the same, for example, for census tract t at hour h, if the result from transportation problem above shows that 10% of its demand is served by substation a and 90% of its demand is served by substation b, then after the adoption of the solar plus storage, its new total demand $d_t^h{}'$ is still served 10% from substation a and 90% from substation b.

Finally, we assign the demand for each substation to its buses proportionally. For instance, for substation a, if its demand before the adoption of the solar plus storage at hour h is O_a^h, and its bus i has demand D_i^h. Then, the new demand for bus i after the adoption of the solar plus storage at hour h, $D_i^h{}'$, is equal to $O_a^h{}' D_i^h / O_a^h$, where $O_a^h{}'$ is the demand for substation a at hour h after the adoption of the solar plus storage.

C. LOAD SHED ANALYSIS

After running the dc load flow with or without the deployment of solar plus storage, the load shed at each bus is determined. Then we can aggregate the load shed from bus-level to substation-level.

To determine the load shed at the census tract level, we allocate the load shed from each substation to each census tract in proportion to the power allocated to the census tract using the modeling process surrounding equations (1)-(4). For example, at hour h, suppose that the load shed for substation k is $L_k^h = \sum_{i \in k} U_i^h$, which is the sum of load shed at each buses inside the substation k, and from the Data Preparation (c2), we know that for census tract t, the amount of power transferred from substation k to census tract t is x_{kt}^h. Then, the load shed for census tract t caused by substation k at hour h, l_{tk}^h, is $L_k^h x_{kt}^h / O_k^h$. Therefore, the total load shed for the census tract is $\sum_k^M l_{tk}^h$ for hour h.

IV. CASE STUDY

The study area includes Los Angeles, Burbank and Glendale illustrated in Fig. 3 and derived from the data included in [48]. Notice that the neighborhoods and cities that suffer more outages in different earthquake scenarios are highlighted on the map. These insights will be described later in this section. The power transmission system of Los Angeles is represented by a network with 432 buses and 545 branches (transmission lines and transformers). The network is analyzed using a dc load flow model at hourly resolution for each period of the 9-period restoration process defined in the previous section under each of the 4,212 consequence scenarios.

For the base case, the 9-period restoration process is assumed to start at June 27, 2030, and continue through August 30, 2030, defining a 65-day restoration process and representing the summer peak. All 9 periods follow the definitions given in the previous section and stem from the HAZUS model. The system-wide demand for each hour during this restoration process was made available by LADWP.

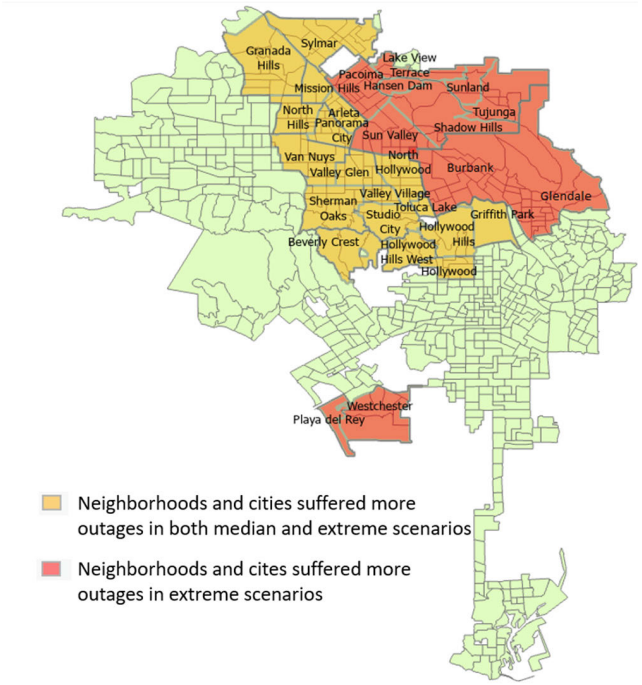

FIGURE 3. Map of los angeles, burbank, and glendale [48].

A. IMPACT OF DAMAGE TO SUBSTATIONS, GENERATORS, AND TRANSMISSION LINES

To understand what components are most important to the restoration process, we explore the 4,212 damage scenarios under seven different cases: (1) all damage specified by the damage scenario is included in the dc load flow model, (2) only substation and generation plant damage is considered, (2) only transmission lines and generation plant damage is considered, (3) only transmission line and substation damage is considered, (5) only transmission line damages is considered, (6) only substation damage is considered, and (7) only generation plant damage is considered. For each case, Fig. 4 shows the log of the annual probability that more than X% of demand will be unserved over the course of the restoration process verses the value of X%.

From Fig. 4, the curve based only on substation damage is quite similar to the *All damage* curve. By contrast, the *Line damage only* curve suggests much lower probabilities of exceeding the same percentage of unserved demand. The generator damage only curve is in between.

This implies that line damage is of little impact when considering load shed across the entire restoration process, and the impact of generation plant damage on demand unserved percentage is substantial but not as substantial as the impact of substation damage. From Fig. 4, we can see that all four functions are very approximately linear on a log-linear plot, which suggests that the distribution of demand unserved follows an approximately exponential distribution.

To explore the demand unserved in each period, box plots for the demand unserved for each period (p1,...,p9) and the entire restoration process (All time) under all seven cases

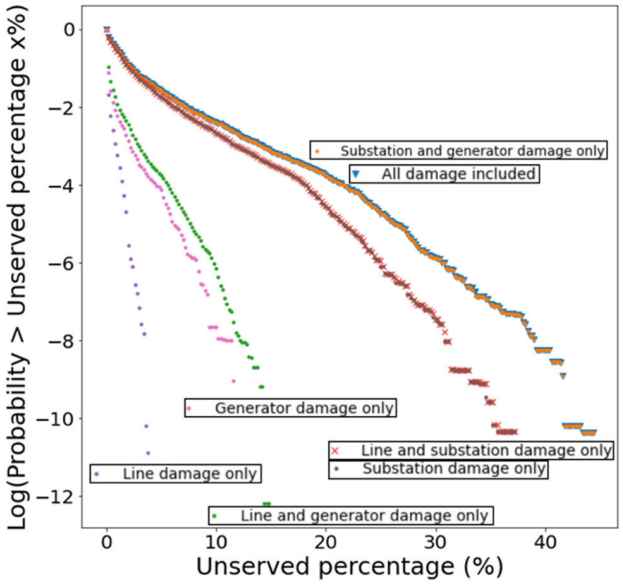

FIGURE 4. Log of probability of exceeding X% demand unserved vs X%, by condition.

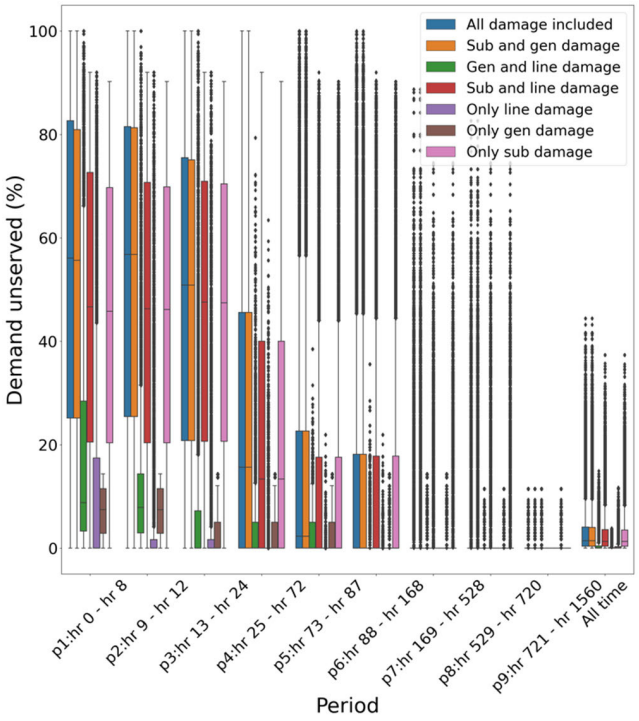

FIGURE 5. Box plot for percentage demand unserved by time period and case.

are shown in Fig. 5. In addition, from Fig. 5, we can see that the percentage demand unserved experiences a significant drop from period 3 to period 4 (at hour 25) when substations with slight damages and transmission lines with moderate damages are repaired. Again, significant drops in demand unserved occur from period 4 to period 5 (at hour 73) when substations with moderate damage and transmission lines with extensive damage are repaired, and from period 6

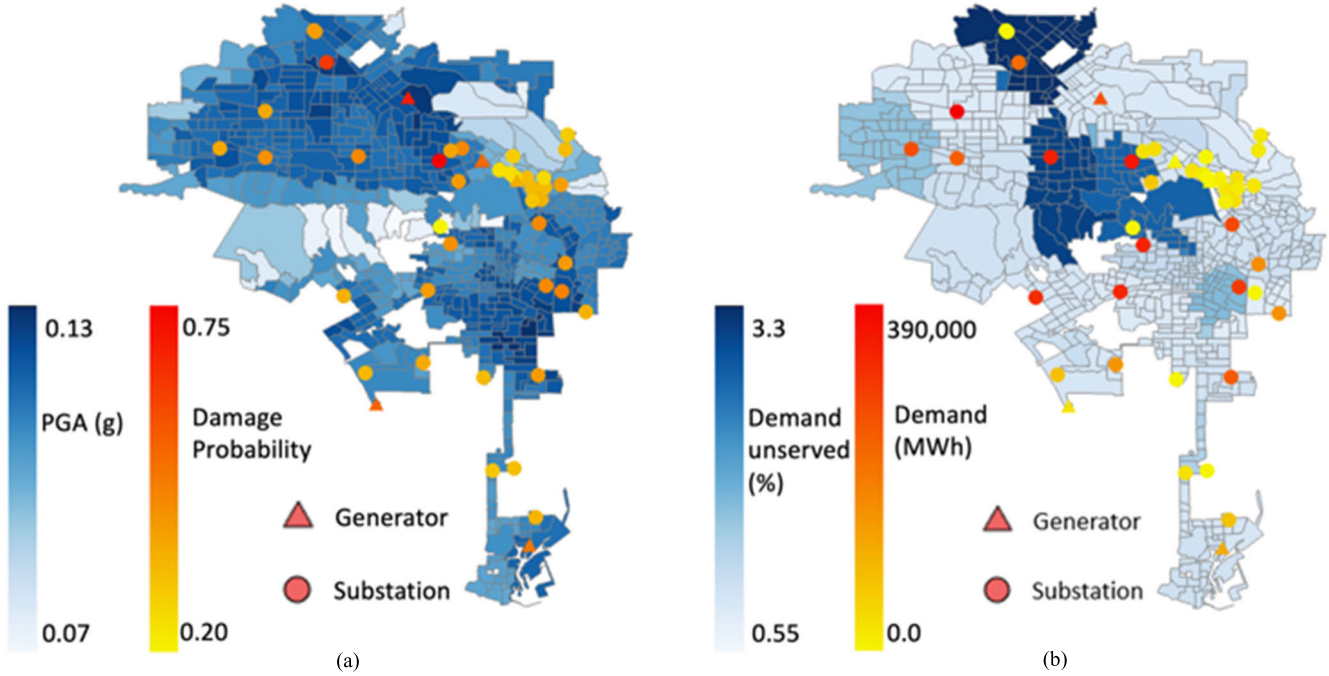

FIGURE 6. Weighted PGA and demand unserved map for median scenarios. (a) PGA map (b) Demand unserved map.

to period 7 (at hour 169) when substations with extensive damage and transmission lines with complete damages are repaired. For the demand unserved percentage over the entire restoration process which is noted as 'All time' in Fig. 5, when all damages are included or only substation and generation plant damage are considered, the average value of demand unserved is around 3.4%. This value implies that on average, 3.4% of power demand in the study area over those 65 days is not supplied by the power transmission system due to the earthquake. However, when only transmission line and generation plant damage is considered, the average value of demand unserved is reduced to 0.6%. What's more, when only transmission line damages are considered, this value reduced to 0.1%.

From Fig. 5 it is important to realize that there are a substantial number of scenarios that place the unserved demand across the 65 days well beyond the mean reaching above 40%. Even for scenarios with smaller values across the 45 days, in the early portions of the restoration process, the load shed can be quite high. These early hours and first days after an earthquake can be very important for life safety and hence the early power disruptions can be very impactful.

B. GEOGRAPHIC PATTERN OF THE LOAD SHED

We consider the geographic pattern in load shed to understand if there are geographic areas that are at higher risk and, if there is a relationship to income or housing tenure type. Hence, we first collect the damage scenarios with system-wide demand unserved between the 40^{th} and 60^{th} percentiles among all 4,212 damage scenarios. Note that this demand unserved percentage value is for the entire study area and full restoration process. We term those scenarios as ''median'' scenarios. We also collect the damage scenarios with demand unserved between the 95^{th} and 100^{th} percentiles among all damage scenarios; we refer to those scenarios as ''extreme'' scenarios.

Fig. 6 (a) and (b) show the weighted average Peak Ground Acceleration (PGA) values and the weighted average percentage demand unserved, respectively, among the median scenarios by census tract. The locations and damage probabilities of each substation and generation plant is plotted on Fig. 6 (a) and the location and the power demand of each substation and generation plant is plotted on Fig. 6 (b). The substations are represented as circles and the generation plants are represented as triangles. From Fig. 6 (a), we can see that the damage probability of substations or generation plants is generally higher at the locations with higher PGA values. Also, the substation and generation plants are generally located in areas that have lower seismic risk.

From Fig. 6 (b), notice that northern and central Los Angeles which include the areas around Van Nuys, Sylmar, North Hollywood, and the Hollywood Hills experience relatively higher levels of average demand unserved in comparison to other areas in the median scenarios. This occurs for two related reasons. First, the two substations supplying power to Sylmar, North Hollywood, and the Hollywood Hills are damaged more frequently across our damage scenarios. The probabilities of damage are 62% and 75% for Sylmar and North Hollywood, respectively. These values are about 20% larger than the next most at-risk substation. For context, the average probability of damage across the other substations

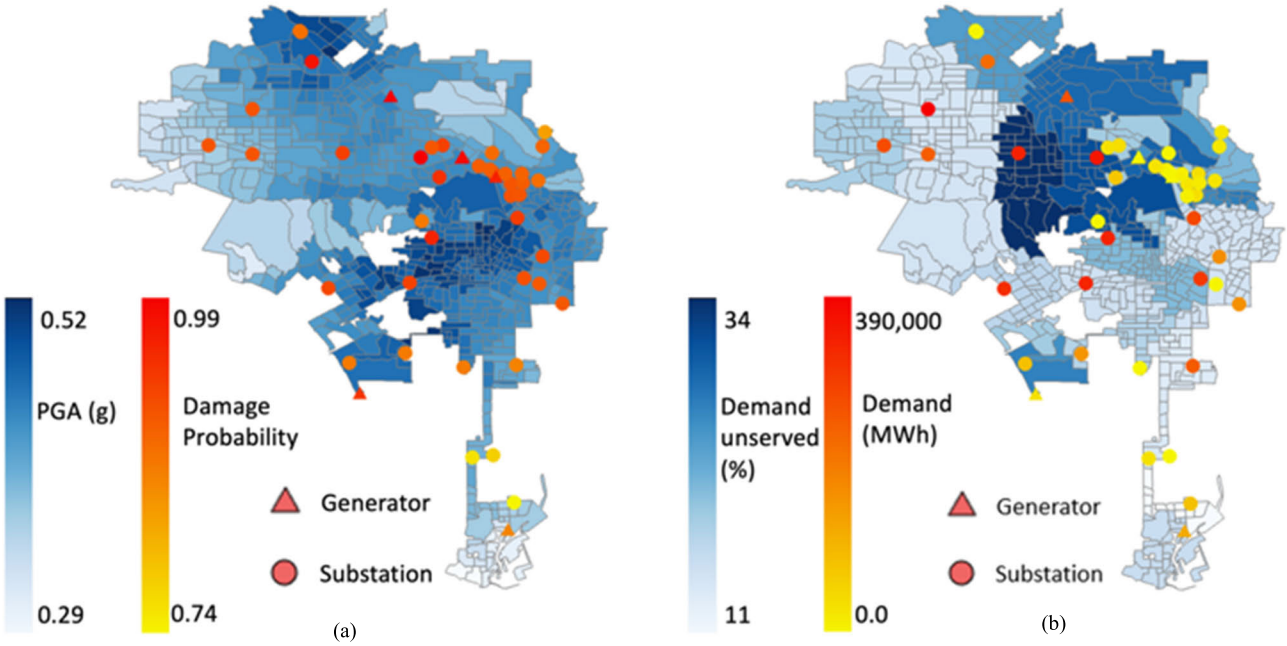

FIGURE 7. Weighted PGA and demand unserved map for extreme scenarios. (a) PGA map (b) Demand unserved map.

is 37%. Further, the probability that the Sylmar and North Hollywood substations experience extensive damage under these median scenarios is 18% and 5%, respectively. The next highest substation's probability of extensive damage is about 3% and it is for the substation that services LAX Los Angeles International Airport. Second, the North Hollywood substation is the only substation supplying power to Van Nuys. Hence, damage to the North Hollywood substation also deenergizes the Van Nuys substation.

It is also important to realize that even small average percentages of demand unserved map to large values in terms of megawatts since the scale of the demand is large. Finally, it is worth noticing that there is a cluster of small substations and generation plants in the Burbank and Glendale areas for which the power demand and damage probability are both lower than others in the study area.

Fig. 7 shows the same two maps for the ''extreme'' scenarios. From Fig. 7 (a), the same results are obtained: higher PGA values are associated with higher damage probabilities, and the locations of substation and generation plants tend to be in areas with relatively lower PGA values. From Fig. 7 (b), it is useful to notice that the areas around Van Nuys, Sylmar, and North Hollywood to the Hollywood Hills, as well as the areas around Tujunga, Sun Valley, LAX airport, Hollywood, Burbank and Glendale suffer relatively more outages than other areas. All substations powering those areas have damage probabilities above 80% with the damage probability for the substation powering North Hollywood to the Hollywood Hills area reaching 99%. More specifically, there is a 60%, 42%, 27%, and 24% probability that the substations powering North Hollywood to Hollywood Hills, Sylmar, Hollywood, and LAX suffer complete damage. Among those areas, the area around Van Nuys, North Hollywood, and LAX have the highest average demand unserved reaching about 34%. (Receiving Station X which will be operational in 2025 and serves the LAX area [49] is included in our study).

C. IMPACT OF ADOPTING SOLAR PLUS STPORAGE

We first create box plots for the demand unserved for each period (p1,. . . ,p9) and the entire restoration process (All time) under three conditions of deployment of solar plus storage in Fig. 8 The first condition is the same as the first condition in Section IV-A, all damage specified by the damage scenarios are included and no solar plus storage is adopted. Under the second condition, all damage specified by the damage scenario is included and the deployment of solar plus storage follows the deployment scenario of SB100, which is the more conservative estimate as mentioned in Section III. Under the third condition, all damage specified by the damage scenario is included and the deployment of solar plus storage follows the deployment scenario of Early & No Biofuels, which assumes a higher adoption rate. From Fig. 8, we can see that adoption of residential customer solar plus storage can reduce the load shed in each period for the entire restoration process. Notice that the first three periods benefit the most from the adoption of solar plus storage. In period 1, the average demand unserved percentage is reduced by about 5% with the deployment scenario of SB100 and by about 9% with the deployment scenario Early & No Biofuels. In period 2, the average demand unserved percentage can be reduced by about 4% with SB100 and by 7% with Early & No Biofuels. In period 3, the average demand unserved percentage is reduced by about 3% with SB100 and by 6% with Early & No Biofuels.

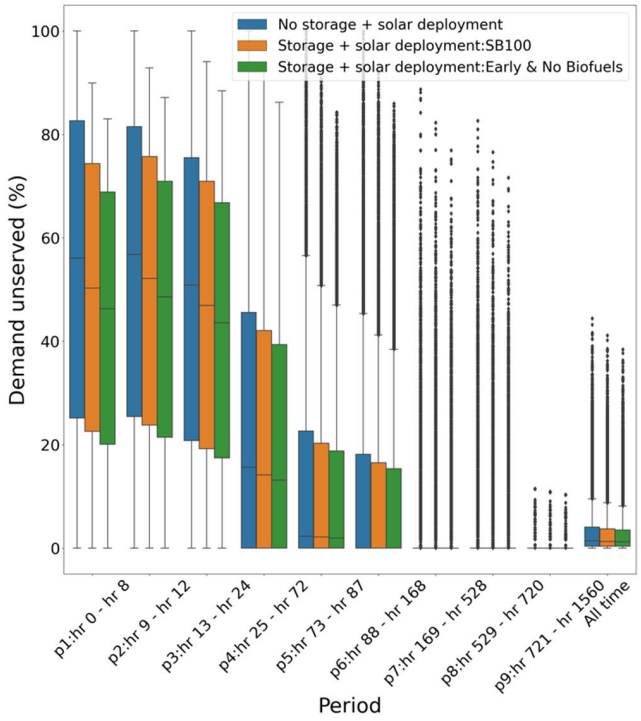

FIGURE 8. Box plot for percentage demand unserved by time period and solar plus storage deployment.

TABLE 1. Sensitivity analysis on percentage of deployment.

Solar plus storage deployment scenarios	Avg. % unserved	Max % unserved	Avg. % unserved extreme scenarios
No deployment	3.38%	44.48%	20.59%
25% of SB100	3.31%	43.65%	20.17%
50% of SB100	3.24%	42.81%	19.75%
75% of SB100	3.17%	41.99%	19.33%
100% of SB100	3.10%	41.20%	18.94%
Early & No Biofuels	2.89%	38.49%	17.62%

We also explore how load shed changes with different percentages of deployment. Table 1 summarizes cases in which we deploy only 25%, 50%, and 75% of solar plus storage capacity under the SB100 deployment scenario. Across those cases, it compares the average demand unserved percentage and maximum demand unserved percentage for all damage scenarios over the entire restoration process, and the average demand unserved percentage for the "extreme" scenarios over the entire restoration process, which is mentioned in section IV-B. Table 1 shows that all three measurements are decreasing proportionally with increasing deployment capacities. Under the SB100 deployment scenario, the average demand unserved percentage for all damage scenarios over whole restoration period and whole study area is reduced by 0.3%, but the maximum demand unserved percentage is reduced by 3.3% and the average demand unserved percentage among extreme scenarios is reduced by 1.6%. If the Early & No Biofuels scenario is applied, the same three measurements can be reduced by 0.5%, 6%, and 3%.

For the geographic pattern of the load shed change after adopting solar plus storage, Fig. 9 shows the weighted average demand unserved percentage among the median scenarios by census tract before and after adopting solar plus storage based on the SB100 deployment scenario. Fig. 9 (a) shows the weighted average demand unserved percentage for census tracts without any solar plus storage adoption, and Fig. 9 (b) shows the weighted average percentage demand unserved percentage map with deployment of solar plus storage under the SB100 deployment scenario. Fig. 9 (c) is the relative benefit map; the relative benefit is defined as the average percentage change in load shed after adopting solar plus storage: 100 × (load shed before deployment-load shed after deployment)/load shed before deployment. From Fig. 9, we can see that the areas suffer higher levels of average demand unserved improve by adopting the solar plus storage as the color becomes lighter. Also, there is one census tract in Sunland which experiences a reduction in average load shed of about 80% after adopting solar plus storage. This occurs because residential demand dominates demand in that census tract, and by adopting the solar plus storage, the residential load shed is reduced significantly. Also from the relative benefit map, we can see that the Bel Air area benefits the most. The pattern of benefit is similar in the extreme scenarios.

D. EFFECT OF EARTHQUAKE TIMING

Since the power demand varies over the year, the timing of the earthquake affects its impact. So far in this paper, and in [13] and [14], the earthquake is assumed to happen during the summer peak load. Now we examine the effect of this timing by recomputing the results when the earthquake happens in the spring, which has the lowest demand in the year. We find that while the amount of load shed is smaller, the percentage load shed is very similar. One reason for this is that most of the earthquake damage is to the substations, and that damage causes a proportional decrease in the load shed. This finding of the same proportional reduction in load shed shows the straightforward way in which the results vary with the earthquake season and allow the extension of all the previous results at peak load to other times of year. The results considering solar plus storage have a similar response to the time of year of the earthquake.

E. EQUIT ISSUES

From the relative benefit map in Fig. 9, we can see that some census tracts benefit more than others from the adoption of solar plus storage. We explore how those benefits are correlated with financial and housing conditions in each census tract. Using the American community survey, we use income information for the 2021 [50] at the study area level.

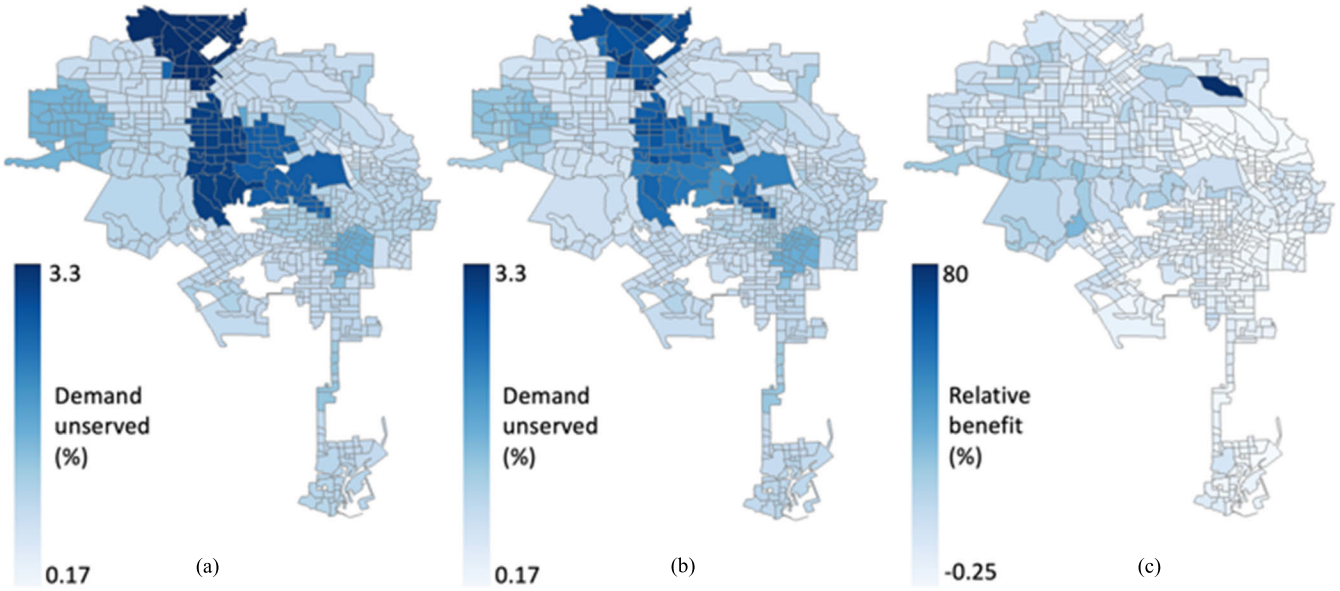

FIGURE 9. Weighted demand unserved percentage before and after adopting solar plus storage for median scenarios (a) Weighted demand unserved before adoption. (b) Weighted demand unserved after adoption. (c) Relative benefit.

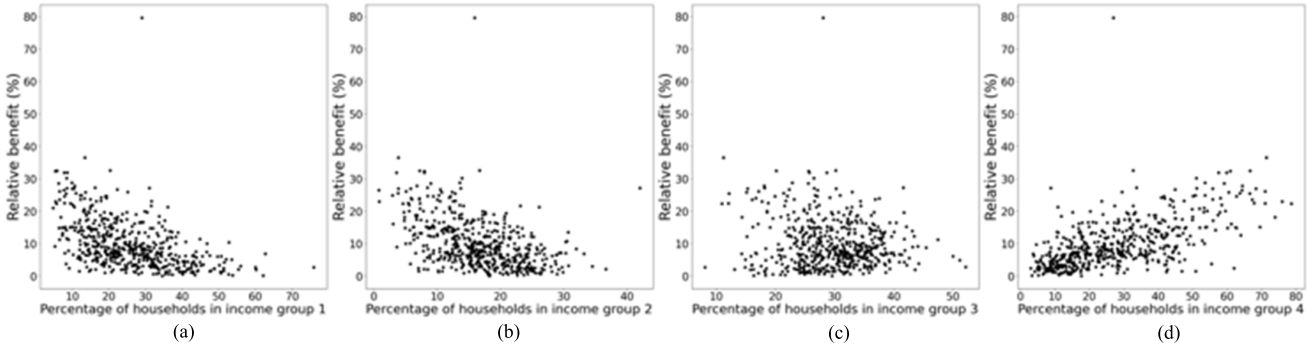

FIGURE 10. Percentage of earning groups vs relative benefit (a) Group 1. (b) Group 2. (c) Group 3. (d) Group 4.

We compute the income associated with the 25th, 50th and 75th percentile. Then, for each census tract, we calculate the percentage of households in each of 4 income groups: (1) lowest quartile, (2) second lowest quartile, (3) second highest quartile, and (4) highest quartile.

First, we explored whether there is a relationship between the average percentage of load unserved by census tract and the percentage of households in each of the four income groups by census tract through a correlation analysis. We find that the correlation between the average percentage load unserved and the percentages of households in each of the four earning groups is sufficiently close to zero to conclude that there is no relationship. In the interest of space, we omit those graphs.

Fig. 10 illustrates the percentage of households in each income group and the relative benefit after adopting solar plus storage by census tract. From Fig. 10 (a) and (b), we see that the relative benefit for census tract has a strong negative linear relationship with the percentage of households in Groups 1 and Group 2. The corresponding correlation coefficients are -0.49 (-0.54 if the outlier census tract is removed) and -0.45 (-0.48 if the outlier census tract is removed), respectively. There is no obvious relationship between the percentage of households in group 3 and the relative benefit. Fig. 10 (d) shows there is a positive linear relationship between the percentage of households in group 4 and the relative benefit. The corresponding correlation coefficient is 0.6 (0.65 if the outlier census tract is removed). Taken together, these correlations demonstrate that households with higher income levels do benefit more under SB100 and that lower-income households benefit less.

The American community survey [51] categorizes housing into owner-occupied and renter occupied. Fig. 11 shows a scatter plot of the percentage of owner-occupied housing and the relative benefit after adopting the solar plus storage by census tract. It confirms there is a positive linear relationship between the percentage of owner-occupied housing and the relative benefit; the corresponding correlation coefficient

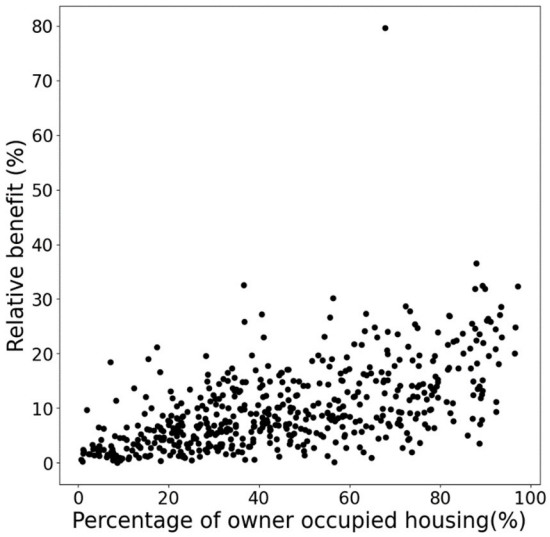

FIGURE 11. The percentage of owner-occupied housing versus the average relative percentage benefit by census tract level.

is 0.56. We also performed the same analysis for the percentage of load unserved and home tenure type and found that there was no relationship. Hence, while there is no relationship between home tenure type and the percentage load shed, there is a relationship between the benefit of storage and rooftop solar and home tenure type under the SB100 deployment scenario.

Furthermore, for each census tract, there is a strong positive linear relationship (corresponding correlation coefficient is 0.7) between the percentage of households in group 4 and the percentage of owner-occupied housing (corresponding correlation coefficient is 0.7). Also, the correlation coefficient between the percentage of households in group 1 and the percentage of owner-occupied housing is -0.7, which reveals a strong negative linear relationship. What's more, the correlation between the percentage of owner occupied housing and multi-unit building density using census tracts yields a corresponding correlation coefficient of -0.66. Taken together, higher levels of owner-occupied housing are associated with higher levels of income and lower multi-unit building density which leads to greater financial ability for adopting solar plus storage and larger per person rooftop area to dedicate to solar power.

V. CONCLUSION

In this study, we explore the vulnerability of the Los Angeles power transmission system to earthquakes and the impact of the adoption of customer-owned solar plus storage on the resilience of the power system after an earthquake. We derive the load shed for each census tract across the restoration period for an earthquake occurring in the summer of 2030 and build on the regional hazard as described in [6] by generating damage scenarios, applying a dc load flow model, and allocating the load shed from substations or generation plants to census tracts. The dc power flow is a simplification of a full ac power flow and looks only at active power flows, neglecting voltage support, reactive power management and transmission losses. Since reactive power management and transmission overloads are not considered in the dc power flow, collectively these can lead to more load shedding. The impacts are quantified of the adoption of customer-owned solar plus storage on the resilience of the power system based on deployment predictions in the LA100 study and performing the same load shed analysis.

This analysis illustrates the importance of substations and secondarily, generation plants to the resilient provision of electric power in Los Angeles. As for the geographic pattern of load shed, the census tracts around Van Nuys, Sylmar, and North Hollywood to Hollywood Hills areas experience relatively higher levels of outages in both the median scenarios and extreme scenarios. Under the extreme scenarios, many more areas experience substantially higher load shed. This analysis assumes that earthquakes occur during the peak summer load. We find that the load shed reduces proportionally if the earthquake is assumed to occur at the minimum load in the spring.

This study also demonstrates that the adoption of customer-owned residential solar plus storage can benefit the restoration process after an earthquake by reducing the load shed in the residential sector. Notice the substantial benefits that occur during the first 3 periods of the restoration process from the adoption of solar plus storage as well the benefits that occur under the more severe earthquake scenarios. Also, since substation damage is the main driver of load shed, the demand change does not affect the average percentage of unserved demand for census tracts with or without solar plus storage; therefore, the absolute value of load shed changes proportionally with the demand change.

We also observe that equity issues do appear to arise in the deployment of customer-owned residential solar plus storage, under the current deployment scenarios. That is, generally, the census tracts with higher levels of higher-income households benefit the most and the census tracts with higher levels of low-income households benefit the least. Additionally, census tracts with higher percentages of owner-occupied housing benefit more than the census tracts with higher percentages of renter-occupied housing. This is because higher levels of renter occupied housing are associated with lower levels of income as well as homes that do not have sufficient roof space per occupant for the same level of storage and solar adoption.

Future research is warranted in two critical areas. First, we used the distance from substation to the census tract to estimate the mapping of census tract demand to substation and generation plant power supply and we assumed no reconfiguration of some of the connections of the distribution system to the substations. This was done because there was no distribution system model available. Second, we only considered customer-owned residential solar plus storage in this study; however, the impact of commercial solar plus storage and utility-owned solar plus storage could be explored.

REFERENCES

[1] X. Dong, N. Shinozuka, and S. Chang, "Utility power network systems," in *Proc. 13th World Conf. Earthq. Eng.*, Vancouver, BC, Canada, Aug. 2004, pp. 1–6.

[2] A. Massie and N. R. Watson, "Impact of the christchurch earthquakes on the electrical power system infrastructure," *Bull. New Zealand Soc. Earthq. Eng.*, vol. 44, no. 4, pp. 425–430, Dec. 2011, doi: 10.5459/bnzsee.44.4.425-430.

[3] A. Suppasri, N. Leelawat, P. Latcharote, V. Roeber, K. Yamashita, A. Hayashi, H. Ohira, K. Fukui, A. Hisamatsu, D. Nguyen, and F. Imamura, "The 2016 Fukushima earthquake and tsunami: Local tsunami behavior and recommendations for tsunami disaster risk reduction," *Int. J. Disaster Risk Reduction*, vol. 21, pp. 323–330, Mar. 2017, doi: 10.1016/j.ijdrr.2016.12.016.

[4] S. Comello, S. Reichelstein, and A. Sahoo, "The road ahead for solar PV power," *Renew. Sustain. Energy Rev.*, vol. 92, pp. 744–756, Sep. 2018, doi: 10.1016/j.rser.2018.04.098.

[5] J. Cochran and P. Denholm, Eds., "The Los Angeles 100% renewable energy study," Nat. Renew. Energy Lab., Golden, CO, USA, Tech. Rep. NREL/TP-6A20-79444., Golden, CO, USA, 2021. [Online]. Available: https://maps.nrel.gov/la100/

[6] N. Soleimani, R. A. Davidson, C. Davis, T. D. O'Rourke, and L. K. Nozick, "Multihazard scenarios for regional seismic risk assessment of spatially distributed infrastructure," *J. Infrastruct. Syst.*, vol. 27, no. 1, Mar. 2021, Art. no. 04021001, doi: 10.1061/(ASCE)IS.1943-555X.0000598.

[7] S. Wolf. *Will Solar Panels Work During a Power Outage?* [Online]. Available: https://www.paradisesolarenergy.com/blog/will-solar-panels-work-during-a-power-outage

[8] Semper Solaris. (2018). *Rooftop Solar Panels and Earthquakes*. [Online]. Available: https://www.sempersolaris.com/rooftop-solar-panels-and-earthquakes/

[9] Federal Emergency Management Agency, *HAZUS Earthquake Model-Technical Manual*, Department of Homeland Security, Washington, DC, USA, Oct. 2020.

[10] T. Anagnos, "Development of an electrical substation equipment performance database for evaluation of equipment fragilities," in *Pacific Gas and Electric and the Pacific Earthquake Engineering Research Center*. Berkeley, CA, USA, Apr. 1999.

[11] I. Vanzi, "Structural upgrading strategy for electric power networks under seismic action," *Earthq. Eng. Struct. Dyn.*, vol. 29, no. 7, pp. 1053–1073, Jun. 2000, doi: 10.1002/1096-9845(200007)29:7<1053::AID-EQE954>3.0.CO;2-X.

[12] Y. Shumuta, "Practical seismic upgrade strategy for substation equipment based on performance indices," *Earthq. Eng. Struct. Dyn.*, vol. 36, no. 2, pp. 209–226, Feb. 2007, doi: 10.1002/eqe.621.

[13] N. R. Romero, L. K. Nozick, I. D. Dobson, N. Xu, and D. A. Jones, "Transmission and generation expansion to mitigate seismic risk," *IEEE Trans. Power Syst.*, vol. 28, no. 4, pp. 3692–3701, Nov. 2013, doi: 10.1109/TPWRS.2013.2265853.

[14] N. Romero, L. K. Nozick, I. Dobson, N. Xu, and D. A. Jones, "Seismic retrofit for electric power systems," *Earthq. Spectra*, vol. 31, no. 2, pp. 1157–1176, May 2015, doi: 10.1193/052112eqs193m.

[15] T. Lagos, R. Moreno, A. N. Espinosa, M. Panteli, R. Sacaan, F. Ordonez, H. Rudnick, and P. Mancarella, "Identifying optimal portfolios of resilient network investments against natural hazards, with applications to earthquakes," *IEEE Trans. Power Syst.*, vol. 35, no. 2, pp. 1411–1421, Mar. 2020, doi: 10.1109/TPWRS.2019.2945316.

[16] B. Cheng, L. Nozick, and I. Dobson, "Investment planning for earthquake-resilient electric power systems considering cascading outages," *Earthq. Spectra*, vol. 38, no. 3, pp. 1734–1760, Aug. 2022, doi: 10.1177/87552930221076870.

[17] A. H.-S. Ang, J. A. Pires, and R. Villaverde, "A model for the seismic reliability assessment of electric power transmission systems," *Rel. Eng. Syst. Saf.*, vol. 51, no. 1, pp. 7–22, Jan. 1996, doi: 10.1016/0951-8320(95)00101-8.

[18] J. A. M. Buriticá Cortés, M. Sánchez-Silva, and S. Tesfamariam, "A hierarchy-based approach to seismic vulnerability assessment of bulk power systems," *Struct. Infrastruct. Eng.*, vol. 11, no. 10, pp. 1352–1368, Oct. 2014, doi: 10.1080/15732479.2014.964732.

[19] A. Poulos, S. Espinoza, J. De la Llera, and H. Rudnick, "Seismic risk assessment of spatially distributed electric power systems," in *Proc. 16th World Conf. Earthq. Eng.*, Santiago, Chile, Jan. 2017, pp. 1949–3029.

[20] B. Johnson, V. Chalishazar, E. Cotilla-Sanchez, and T. K. A. Brekken, "A Monte Carlo methodology for earthquake impact analysis on the electrical grid," *Electr. Power Syst. Res.*, vol. 184, Jul. 2020, Art. no. 106332, doi: 10.1016/j.epsr.2020.106332.

[21] A. M. Salman and Y. Li, "A probabilistic framework for seismic risk assessment of electric power systems," *Proc. Eng.*, vol. 199, pp. 1187–1192, Jan. 2017, doi: 10.1016/j.proeng.2017.09.324.

[22] S. Espinoza, A. Poulos, H. Rudnick, J. C. de la Llera, M. Panteli, P. Mancarella, R. Sacaan, A. Navarro, and R. Moreno, "Seismic resilience assessment and adaptation of the northern Chilean power system," in *Proc. IEEE Power Energy Soc. Gen. Meeting*, Chicago, IL, USA, Jul. 2017, pp. 1–5, doi: 10.1109/PESGM.2017.8274288.

[23] M. Nazemi and P. Dehghanian, "Seismic-resilient bulk power grids: Hazard characterization, modeling, and mitigation," *IEEE Trans. Eng. Manag.*, vol. 67, no. 3, pp. 614–630, Aug. 2020, doi: 10.1109/TEM.2019.2950669.

[24] R. Weinmann, E. Cotilla-Sanchez, and T. Brekken, "Toward models of impact and recovery of the U.S. western grid from earthquake events," *Energies*, vol. 15, no. 24, p. 9275, Dec. 2022, doi: 10.3390/en15249275.

[25] M. Shinozuka, X. Dong, X. Jin, and T. C. Cheng, "Seismic performance analysis for the ladwp power system," in *Proc. IEEE/PES Transmiss. Distrib. Conf. Expo., Asia Pacific*, Dalian, China, Aug. 2005, pp. 1–6, doi: 10.1109/TDC.2005.1547165.

[26] Z. Çağnan, R. A. Davidson, and S. D. Guikema, "Post-earthquake restoration planning for Los Angeles electric power," *Earthq. Spectra*, vol. 22, no. 3, pp. 589–608, Aug. 2006, doi: 10.1193/1.2222400.

[27] M. Shinozuka, X. Dong, T. C. Chen, and X. Jin, "Seismic performance of electric transmission network under component failures," *Earthq. Eng. Struct. Dyn.*, vol. 36, no. 2, pp. 227–244, Jan. 2007, doi: 10.1002/eqe.627.

[28] N. Xu, S. D. Guikema, R. A. Davidson, L. K. Nozick, Z. Çağnan, and K. Vaziri, "Optimizing scheduling of post-earthquake electric power restoration tasks," *Earthq. Eng. Struct. Dyn.*, vol. 36, no. 2, pp. 265–284, Feb. 2007, doi: 10.1002/eqe.623.

[29] A. Sarreshtehdari, N. Elhami Khorasani, and M. Coar, "A streamlined approach for evaluating post-earthquake performance of an electric network," *Sustain. Resilient Infrastruct.*, vol. 5, no. 4, pp. 232–251, Jan. 2019, doi: 10.1080/23789689.2018.1542211.

[30] D. Ding, W. B. Leigh, and X. Wang, "Simulation of earthquake damage on rooftop photovoltaic systems," in *Proc. 11th U.S. Nat. Conf. Earthq. Eng., Integrating Sci., Eng. Policy*, Los Angeles, CA, USA, Jun. 2018.

[31] S. E. M. Walters and J. Baker, "Seismic considerations and evaluation approach for 'isolated' rooftop PV arrays," in *Proc. SEAOC Convention*, Santa Fe, NM, USA, 2012, pp. 1–13.

[32] L. Ceferino, C. Liu, I. Alisjahbana, S. Patel, T. Sun, A. Kiremidjian, and R. Rajagopal, "Earthquake resilience of distributed energy resources," in *Proc. 17th World Conf. Earthq. Eng.*, Tokyo, Japan, 2020, pp. 1–9.

[33] S. Patel, L. Ceferino, C. Liu, A. Kiremidjian, and R. Rajagopal, "The disaster resilience value of shared rooftop solar systems in residential communities," *Earthq. Spectra*, vol. 37, no. 4, pp. 2638–2661, Nov. 2021, doi: 10.1177/87552930211020020.

[34] R. Artis, M. Assili, and M. Shivaie, "A seismic-resilient multi-level framework for distribution network reinforcement planning considering renewable-based multi-microgrids," *Appl. Energy*, vol. 325, Nov. 2022, Art. no. 119824, doi: 10.1016/j.apenergy.2022.119824.

[35] E. Galvan, P. Mandal, and Y. Sang, "Networked microgrids with roof-top solar PV and battery energy storage to improve distribution grids resilience to natural disasters," *Int. J. Electr. Power Energy Syst.*, vol. 123, Dec. 2020, Art. no. 106239, doi: 10.1016/j.ijepes.2020.106239.

[36] P. Gautam, P. Piya, and R. Karki, "Resilience assessment of distribution systems integrated with distributed energy resources," *IEEE Trans. Sustain. Energy*, vol. 12, no. 1, pp. 338–348, Jan. 2021, doi: 10.1109/TSTE.2020.2994174.

[37] J. Guenaou, P. Henneaux, and D. S. Kirschen, "Impact of distributed energy resources on power system resilience against earthquakes," in *Proc. IEEE PES Innov. Smart Grid Technol. Conf. Eur. (ISGT-Europe)*, Novi Sad, Serbia, Oct. 2022, pp. 1–5, doi: 10.1109/ISGT-Europe54678.2022.9960485.

[38] S. D. Guikema, R. Nateghi, S. M. Quiring, A. Staid, A. C. Reilly, and M. Gao, "Predicting hurricane power outages to support storm response planning," *IEEE Access*, vol. 2, pp. 1364–1373, 2014, doi: 10.1109/ACCESS.2014.2365716.

[39] D. B. McRoberts, S. M. Quiring, and S. D. Guikema, "Improving hurricane power outage prediction models through the inclusion of local environmental factors," *Risk Anal.*, vol. 38, no. 12, pp. 2722–2737, Oct. 2016, doi: 10.1111/risa.12728.
[40] N. J. K. Brown, J. L. Gearhart, D. A. Jones, L. K. Nozick, N. Romero, and N. Xu, "Optimizing the selection of scenarios for loss estimation in transportation networks," in *Proc. Winter Simulation Conf.*, Phoenix, AZ, USA, Dec. 2011, pp. 1–12.
[41] D. A. Swanson, A. Schlottmann, and B. Schmidt, "Forecasting the population of census tracts by age and sex: An example of the Hamilton–Perry method in action," *Population Res. Policy Rev.*, vol. 29, no. 1, pp. 47–63, Feb. 2010, doi: 10.1007/s11113-009-9144-7.
[42] U.S. Census Bureau. (2010). *2006–2010 Age and Sex. American Community Survey 5-Year Estimates*. [Online]. Available: https://data.census.gov/table?t=Age+and+Sex&g=0500000US06037$1400000&y=2010
[43] U.S. Census Bureau. (2020). *2016–2020 Age and Sex. American Community Survey 5-Year Estimates*. [Online]. Available: https://data.census.gov/table?t=Age+and+Sex&g=0500000US06037$1400000&y=2020
[44] U.S. Census Bureau. (2020). *2016–2020 Industry by Sex for the Civilian Employed Population 16 Years and Over. American Community Survey 5-Year Estimates*. [Online]. Available: https://data.census.gov/table?t=Industry&g=050XX00US06037$1400000&y=2020&tid=ACSST5Y2020.S2403
[45] H. Goldstein, "Projecting state and area industry employment," Produced Projections Workshop, Employment Training Admin., U.S. Dept. Labor, Washington, DC, USA, 2005.
[46] Caltrans. (2021). *Los Angeles County Economic Forecast*. [Online]. Available: https://dot.ca.gov/programs/transportation-planning/division-of-transportation-planning/data-analytics-services/transportation-economics/long-term-socio-economic-forecasts-by-county
[47] Californian Energy Commission. (2021). *SB 100 Joint Agency Report*. [Online]. Available: https://www.energy.ca.gov/sb100
[48] City of Los Angeles Hub. *LA Times Neighborhood Boundaries*. [Online]. Available: https://geohub.lacity.org/datasets/d6c55385a0e749519f238b77135eafac/explore?location=34.019242%2C-118.424709%2C10.67
[49] LAWA. *Receiving Station X*. [Online]. Available: https://www.lawa.org/transforminglax/projects/underway/rsx#:~:text=In%20cooperation%20with%20the%20Los,Angeles%20International%20Airport%20(LAX)
[50] U.S. Census Bureau. (2021). *2017–2021 Income in the Past 12 Months (in 2021 Inflation-Adjusted Dollars). American Community Survey 5-Year Estimates*. [Online]. Available: https://data.census.gov/table?t=Income+(Households,+Families,+Individuals)&g=0500000US06037$1400000&y=2021&tid=ACSST5Y2021.S1901
[51] U.S. Census Bureau. (2021). *2017–2021 Tenure American Community Survey 5-Year Estimates*. [Online]. Available: https://data.census.gov/table?t=Owner/Renter+(Tenure)&g=0500000US06037$1400000&y=2021&tid=ACSDT5Y2021.B25003

BOYU CHENG received the B.S. degree in civil engineering from Purdue University, in 2016, the M.S. degree in civil engineering from Georgia Institute of Technology, in 2018, and the Ph.D. degree in civil engineering from Cornell University, in 2023. His research interest includes the simulation of civil infrastructure under natural hazards.

LINDA NOZICK (Member, IEEE) received the B.S.E. degree in systems analysis and engineering from George Washington University, in 1989, and the M.S.E. and Ph.D. degrees in systems engineering from the University of Pennsylvania, in 1990 and 1992, respectively. She is currently a Professor of systems engineering with Cornell University. Her research interests include math modeling to address problems in infrastructure and disaster mitigation.

IAN DOBSON (Life Fellow, IEEE) received the B.A. degree in mathematics from Cambridge University, U.K., and the Ph.D. degree in electrical engineering from Cornell University, Ithaca, NY, USA. He was with British industry and the University of Wisconsin–Madison, USA. He is currently a Sandbulte Professor of electrical engineering with Iowa State University, Ames, IA, USA. His research interests include power system resilience, blackout risk, cascading failure, complex systems, and nonlinear dynamics.

RACHEL DAVIDSON received the B.S.E. degree in civil engineering from Princeton University and the M.S. and Ph.D. degrees in civil engineering from Stanford University. She is currently an Associate Dean for Academic Affairs with the College of Engineering, a Professor with the Department of Civil and Environmental Engineering, and a core Faculty Member with the Disaster Research Center, University of Delaware. Her research interests include natural disaster risk modeling and civil infrastructure systems.

DENIS OBIANG received the joint B.S.E. degree in electrical engineering from California Polytechnic State University and the University of California, in 2005, and the M.S.E. degree in electrical engineering from the University of California Los Angeles, in 2009, with a focus on microchip design. He is currently the Director of power system planning with Los Angeles Department of Water and Power.

JOSÉ DIAS (Member, IEEE) received the B.S. and M.S. degrees in electrical engineering from California State University, Los Angeles, in 2005 and 2009, respectively. He is currently with Los Angeles Department of Water and Power. He is also a supervisor of western transmission planning overseeing affected system interconnection studies and participating in regional transmission planning.

MICHAEL GRANADOS received the B.S. degree in electrical engineering from California State Polytechnic University, Pomona, in 2017. He is currently with Los Angeles Department of Water and Power, specializing in power system analysis, transmission planning, and production cost modeling.